Results in Engineering 24 (2024) 103563

Contents lists available at ScienceDirect

Results in Engineering

journal homepage: www.sciencedirect.com/journal/results-in-engineering

RLS adaptive filter co-design for de-noising ECG signal

Ahlam Fadhil Mahmood [a], Safaa N. Awny [b], Ali Alameer [c,*]

[a] Department of Computer Engineering, University of Mosul, Iraq
[b] College of Pharmacy, University of Mosul, Iraq
[c] School of Science, Engineering and Environment, University of Salford, UK

ARTICLE INFO

Keywords:
Electrocardiogram
Adaptive algorithm
Co-design
FPGA
Soft processor

ABSTRACT

Doctors diagnose various heart muscle disorders by continuously analyzing ELECTROCARDIOGRAM (ECG) signals. Obtaining a noise-free ECG recording is difficult due to various types of interference, making an effective filter essential for accurate diagnosis. This paper introduces a novel, low-complexity filter designed to enhance ECG signal quality. The proposed method involves partitioning the implementation of the Recursive Least Squares (RLS) adaptive filter between a Microblaze soft processor and hardware resources within a Field Programmable Gate Array (FPGA). The hardware component is responsible for creating a Finite Impulse Response (FIR) filter, while the adaptive processing is handled by the soft processor. This configuration makes the filter adaptable, allowing it to work with various algorithms for a wide range of applications. The co-design was tested for ECG noise removal, achieving an average Signal-to-Noise Ratio (SNR) improvement of 89.78 %. Offloading adaptive tasks to the soft processor reduced power consumption by 56.2 %, making it suitable for integration with ECG sensors in wearable body networks.

1. Introduction

Cardiovascular diseases pose a serious threat to human health. The World Heart Federation expects more than 23 million deaths annually for cardiovascular patients by 2030, according to a report (World Heart Federation, 2019) [1]. Given the rapid growth of aging in the world, the diagnosis and treatment of cardiovascular diseases is a global necessity, especially because most injuries occur in middle-aged and elderly people [2–5]. An ELECTROCARDIOGRAM (ECG) is a diagnostic instrument for various cardiac and blood disorders. Reading ECG signals provides real-time heart rhythm analysis, heart rate variability, cardiac ischemia, and the detection of respiratory abnormalities [6]. As shown in Fig. 1, the ECG has different features (P, Q, R, S, T, and U) of varying intervals (P-R, QRS, etc.) known to physicians to determine the heart's health. It is a low amplitude signal ranging from 0.5 mV to 5 mV, with a frequency of 60 to 80 pulses susceptible to many types of noises [7].

Since the ECG signal has low amplitude/frequency waves, it is very sensitive to noise, whether internal or external, high or low frequency. Among the types of impacting noise are electromyography noise (EMG) or muscle, artifacts (MA), and line wandering (BW) noise [8–12], etc. Each type has characteristics that affect the diagnosis of the electrocardiogram, and the following are the most important types and their features:

1.1. Power line interference (PLI)

PLI is a stationary interference caused by the capacitive and inductive coupling of 50/60 Hz power lines in the ECG acquisition circuit [14–16]. PLI lower frequencies are merged with the ECG signal. This interference leads to the destruction of P-waves, which causes an incorrect verdict of atrial arrhythmias such as fibrillation and atrial hypertrophy [7].

1.2. Base line wandering (BLW)

It is a low-frequency artifact produced mainly by patient movement, poor contact with electrodes, and changes in skin-electrode impedance. Frequently, when measuring with a wearable ECG sensor while performing exercises or in an ambulance. [17–18]. This baseline drift is as high as around 15 % of the peak-to-peak ECG amplitude over the 0.15–0.3 Hz frequency range. These artifacts distort the ST segment as well as other ECG low-frequency components. This ST-segment misrepresentation may cause an incorrect diagnosis of Brugada syndrome, myocardial infarction, and many other related anomalies [16].

* Corresponding author.
E-mail addresses: ahlam.mahmood@uomosul.edu.iq (A.F. Mahmood), safaanawny@uomosul.edu.iq (S.N. Awny), A.Alameer1@salford.ac.uk (A. Alameer).

https://doi.org/10.1016/j.rineng.2024.103563
Received 20 December 2023; Received in revised form 19 November 2024; Accepted 26 November 2024
Available online 28 November 2024

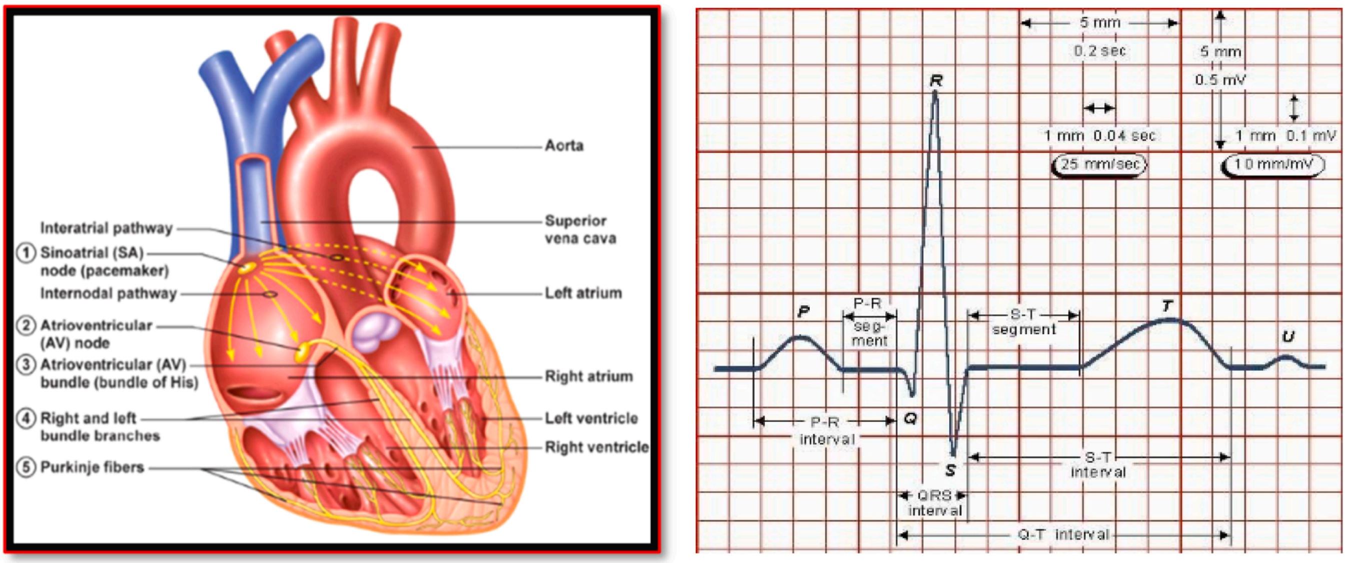

Fig. 1. Anatomy of the cardiovascular system and ECG signal [13].

1.3. Muscle artifacts (MA)

This type of electrical activity is generated in the muscles when one of them moves, especially those close to the head, such as the movement of the neck or eyes, and when swallowing, as well as from the heartbeat [7]. These activities, owing to muscle shrinkages, last for approximately 50ms between (0 and 10,000 Hz), with an amplitude of around 10 % of the full-scale deflection [17]. This noise distorts the ECG waves because it has a frequency of 0.01 to 100 Hz. They hinder the correct identification of heart rate disorders, especially in wearable systems [18–20]. The design of wearable portable devices must consider the impact of physical activities such as shifting between sitting and standing, running, climbing stairs, etc., which present a major challenge to achieving correct readings.

1.4. Channel noise

Sending ECG over a channel with poor conditions, such as Additive white Gaussian noise (AWGN) or any other type, corrupts it.

1.5. Miscellaneous noises

It is a mixture of electrode motion artifacts EMA, MA, and BLW [7], or a mixture of BLW, EMA, PLI, and MA [14,16]. In addition, any other combination that leads to a change in the peak amplitude, duration, and spectrum range causes a misdiagnosis of the ECG signal.

2. Literature review

Electrocardiogram contamination is an ongoing problem that affects the results of its analysis. Deformation may occur at the following stages: acquisition, processing, or transfer. In general, effective treatment of the noise problem contributes to obtaining an accurate diagnosis from the electrocardiogram. Many de-noising techniques are available in the works of literature, one of them begins the threshold processing procedure, which is a common way of removing noises by exploring the global and local signal characteristics [15,21–22]. Besides using wavelet transform methods to reduce ECG noise by analyzing the signal, determining the threshold type, and reconstructing the signal [23–26]. Another category is based on deep learning strategies, which target regenerating a pure ECG signal from a besmirched signal by optimizing the objective function [27–30]. Another important ECG de-noising category is using Bayesian filters to evaluate variations in the ECG dynamic model by adaptive filters [31–33]. A hybrid strategy is the last category that combines the different procedures such as wavelet and smoothing filter [34] and combines the multiresolution wavelet nature with the adaptive learning capability of artificial neural networks [35]. Table 1 summarizes notable solutions written in the literature and emphasizes their main contributions.

From the literature, it is clear the importance of using RLS as the most appropriate filter to cancel ECG noise, but the stumbling block is the great computational complexity of the filter, as its implementation requires (N^2+5N+1) multiplier and (N^2+3N) addition, in addition to the division process. Overcoming this complexity is the most important goal of this paper.

The main contribution of this paper is to propose a new design for an RLS filter that is better for filtering the ECG signal while overcoming its great complexity by partitioning its work between the FPGA components. This enabled the design to work on removing various noises with high accuracy. Giving the task of completing complex calculations to the MicroBlaze processor without hardware building reduces the complexity and consumption. The proposed design can easily work with any other algorithm and for various applications.

The remainder of this manuscript is arranged as follows: Section 3 explains materials and methods using adaptive RLS equations and techniques. Section 4 demonstrates the benefits of co-design, linking the soft processor and the hard tools parts, and the software platform for merging HW/SW. Experimental analysis is discussed in Section 5 with an SNR of different noise types. Section 6 presents the conclusion and suggestions.

3. Martial and methods

Requiring an accurate ECG is the main motivation for much of the research. The ability to work in anonymous and varying environments has made the adaptive filter an effective tool for heart signal filtration. Continuously adaptive filters adjust their weights using the adaptive algorithm for error minimization. In general, the least mean square (LMS), Normalized LMS (NLMS), and Recursive Least Squares (RLS) are the most standard sets of adaptive algorithms [36]. RLS procedure provides the best results compared to LMS and NLMS algorithms with superior convergence rate and shorn of any adjustment of its parameters [37], but it needs high calculation and memory with increasing the signal sampling rate and filter order. RLS is excellent for working in

Table 1
Summary of the de-noising ECG in the reviewed articles

Ref.	Procedure	Result	Tool/dataset	Advantages	Disadvantages
[6]	Motion artifact, compared with: (FIR[1], Zero-phase IIR[2], moving average, moving median) filters, wavelet, empirical mode decomposition, and adaptive filter.	Adaptive filtering has a better SNR.	MATLAB software/ clean ECG and with BLW noise from the MIT-BIH	Recording the ECG and impedance pneumography signals by using special design hardware.	Reducing motion artifact only.
[8]	De-noising the left-arm ECG from a wearable device using LMS, RLS, and extended kernel RLS.	Maximal SNR, PLI removing by utilizing RLS adaptive filter (step size $= 1\times10^{-5}$), named (T-ECG).	MATLAB/ MIT-BIH	Different noises with various step sizes. T-ECG: available at https://github.com/rafa-coding-projects/T-ECG	Not declare the tap length. Taking step size only without other RLS parameters.
[9]	Proposed a 12-layer-1D-CNN to classify five classes of heartbeat with wavelet self-adaptive threshold. The results were compared with those of the BP neural network, RF[3], and other CNN networks.	CNN performance Accuracy= 97.41%, Sensitivity= 97.05%, Specificity= 99.35%, and the positive prediction rate =97.21%.	MATLAB DL[4] Toolbox trained on an Intel i5-7300 HQ PC, 16GB-RAM, and TX1050 as GPU. /MIT-BIH database	Classify five classes: [normal (NOR), left bundle branch block (LBBB), right bundle branch block (RBBB), Atrial premature beats (AP), and premature ventricular beats (PVC)]. Data: https: //physionet.org/content/mitdb/1.0.0/	Anti-noise capability without stating different ECG noise types.
[11]	Contributed to a determination of adaptive threshold procedure based on the 3σ[5] standard.	Improve SNR of six synthetic ECGs (Syn00-Syn05) with the original SNRs of (-2, -5, 2, 5, 10) dB. Best performance with the highest average SNR.	MATLAB 2016/MIT-BIH database using 3-noise type [BLW, EM, and MA contain muscle artifacts].	Study different noises: electromyogram noise (EMG), baseline wandering (BW), electrode contact noise (ECN), white noise (WN), and hybrid noise (HN).	An adaptive threshold maintained the QRS information and de-noised the ECG diagram.
[15]	Investigated a dual-tree CWT[6] based on threshold tuning to deliver de-noising ECG. Eight threshold sets were tested to obtain the best threshold function.	The best results (80.72 SNR) were obtained with a proposed estimator with 23 minimization factors and a normal distribution.	MATLAB R2016 Intel Corei5, using 64bit OS/ MIT-BIH arrhythmia V5 of 100 records, is derivative from the Physio-ATM.	Different threshold processes [Hard, Soft, Non-negative garrote, Trimmed, Hyperbolic, and Semi-soft]. Comparing different distributions (Normal, and Gaussian).	Removing only the baseline wander noise.
[23]	FPGA[7] design for de-noising the ECG signal to improve ventricular late potentials (VLP) detection based on WT[8]. Their system has been realized on Altera's FPGA and confirmed on the DE1-SoC[9].	The probability density functions of the vector magnitude values in the presence of delayed ventricular potentials are plotted in Fig. 6 of [23].	MATLAB and Quartus-II 14.1 software	Hard threshold on the 3-detail levels, and four levels are added. FPGA hardware realization. State the IIR and FIR filter coefficients. Comparing MATLAB values with the simulation results.	Focused attention is paid to the hardware implementation without mentioning how much noise is reduced, especially since it is designed to operate in real time.
[27]	6-filters [Median, Gaussian, Moving Average, Savitzky–Golay, Low-Pass Butter, and Wavelet De-noising] are compared with Custom CNNs. Presented three 1D-CCNN[10] models: (Model-1, Model-2) consisting of 5-CLs[11], 5-max-pooling layers, and 1-fully connected layer. (Model-3) consists of 4-CLs, 4-fully connected layers, 3-max-pooling layers, max-pooling, and dropout alternating each other in the models.	PSNR of 6-filters are [87.3, 86.5, 81.05, 80.5, 78.6, 56.9]. CCNN: Model-1 reached accuracy= 93.03%, sensitivity= 52.18%, and specificity= 84.45%. For Model-2 accuracy= 89.03%, sensitivity= 47.92%, and specificity= 95.88%. While. Model-3 achieved accuracy= 89.56%, sensitivity= 47.48%, and specificity= 87.20%.	Python (Scipy library), Google collab with Tesla K80 GPU, CPU Intel, Xenon(R), RAM 13 Gb/(MIT-BIH Arrhythmia and Boston's Beth Israel Hospital). 80% training, and 20% for testing.	The median filter has a higher PSNR[12]. CCNN architecture can help doctors accurately diagnose coronary artery illness.	Not studying different noise types. Small dataset, Filtering results in PSNR and CCNN in different parameters that cannot be compared.

Note: FIR[1]: finite impulse response, IIR[2]:infinite impulse response, RF[3]: Random Forest, DL[4]: Deep Learning, σ[5]: Standard deviation of the intrinsic mode functions, CWT[6]: Complex Wavelet Transform, FPGA[7]: Field Programmable Gate Array, WT[8]:wavelet transform, DE1-SoC[9](Development and Evaluation board-System-on-Chip), 1D-CCNN[10]=one-dimension Complex Convolutional Neural Networks, CL[11]: Convolution Layers, PSNR[12]:: Peak-Signal-to-Nise Ratio.

non-stationary environments while ignoring the computational complexity, especially when used for de-noising the ECG signal. The RLS algorithm contains recursive updating of the $\omega(n)$ and the inverse autocorrelation $P(n)$ matrix. $k(n)$ gain evaluation and the inverse autocorrelation matrix P(n), are required to calculate the product as follows [38]. The related equations of the RLS adaptive are as follows: -

$$\omega(n) = [\omega_0(n)\ \omega_1(n)\ \omega_2(n)\ \ldots\ \omega_{N-1}(n)]^T, \tag{1}$$

$$x(n) = [x(n)\ x(n-1)\ \ldots x(n-N+1)]^T, \tag{2}$$

$$y(n) = \omega^T(n-1)\ x(n), \tag{3}$$

$$e(n) = d(n) - \ y(n), \tag{4}$$

$$k(n) = \frac{\lambda^{-1}P(n-1)x(n)}{1+\lambda^{-1}x^T(n)P(n-1)x(n)}, \tag{5}$$

$$P(n) = \lambda^{-1}\{P(n-1) - k(n)x^T(n)P(n-1)\}, \tag{6}$$

$$\omega(n) = \omega(n-1) + k(n)\ e(n), \tag{7}$$

where ω(n) is the weight vector, N is the filter length, and x(n) represents the input s. d(n) is the desired signal, e(n) demonstrates the output noise, and the correlation matrix $\boldsymbol{P}(0) = \delta^{-1}$I where δ is a small positive constant. In addition, λ denotes the forgetting factor ($0 << \lambda \leq 1$) and $\lambda \in (0, 1)$.

The RLS adaptive filter provides a better adaptive solution to remove various noises from the ECG signals. Despite having better convergence

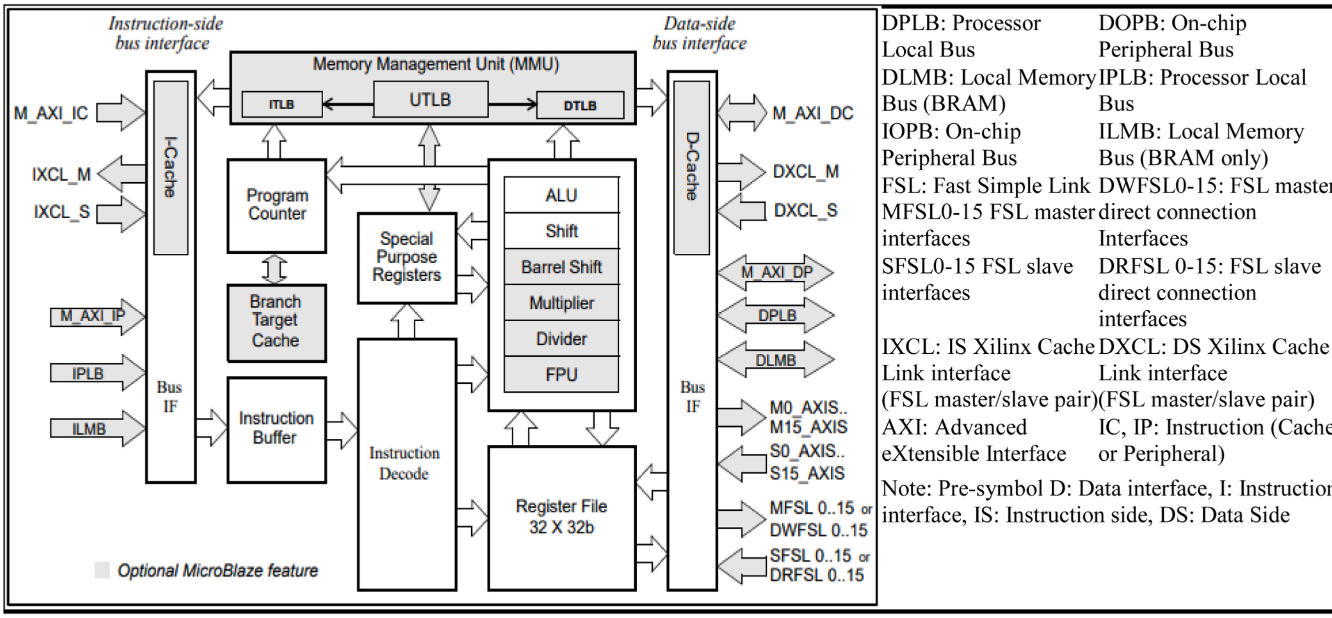

Fig. 2. Internal schematic diagram of a Microblaze™ Xilinx soft processor with signals interfaces and busses indicated [42].

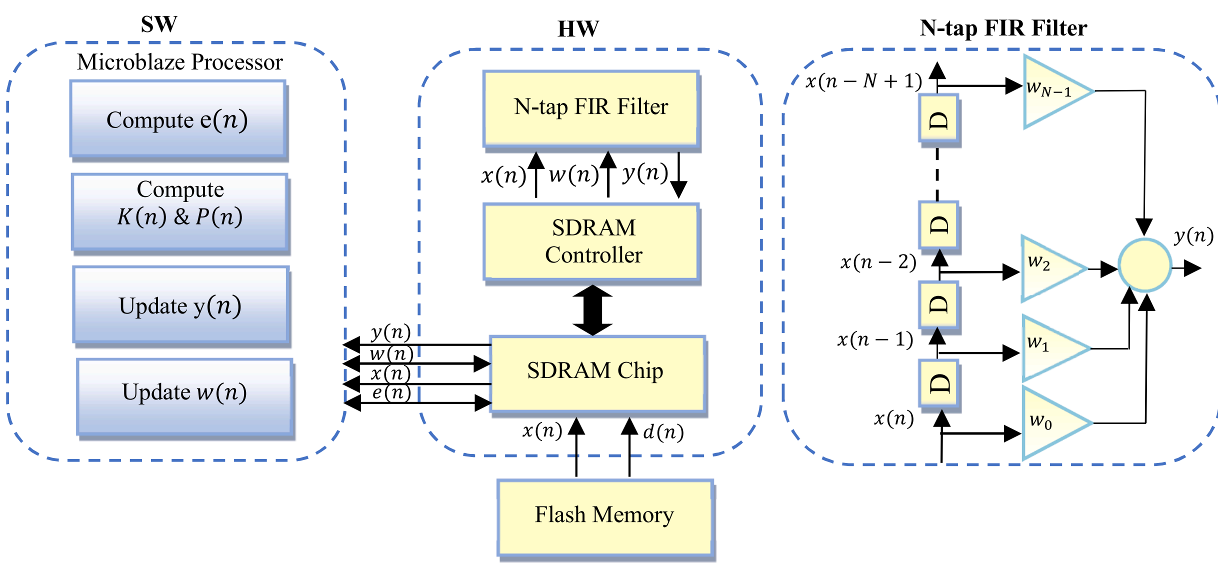

Fig. 3. Architecture of the proposed Co-design RLS Filter (hardware FIR filter and adaptation with Microblaze soft processor).

and parameter tracking ability, the RLS algorithm requires expensive computational resources and sometimes suffers from numerical stability issues. Soft programming cooperation with hardware resources represents an essential solution to this problem; if the microprocessor is programmed to perform an adaptive RLS task, then the simple FIR components can achieve the RLS task without complexity. Their parameters are updated depending on the output calculations of the microprocessor. The main contribution of this paper is to propose a collaboration between hardware and software to accomplish the adaptive RLS task, which is challenging when built with hardware only.

4. The proposed RLS co-design

Currently, FPGA vendors use System-on-chip (SoC) devices that involve one or more soft/hard processors and an FPGA printed on a single circuit for designing more complex systems. Virtex 5 FPGA is one of the gate arrays of the Xilinx family [39]. Xilinx ML506 evaluation platform contains a Microblaze™ soft embedded processor, which is a 32-bit reduced instruction set computer (RISC) [40–42]. It was constructed with Harvard architecture which isolates data storage memory and instruction memory as shown in Fig. 2. Collaboration between software engineers and hardware designers (co-design), has revolutionized many aspects of traditional FPGA hardware, by making it freer. This flexibility is also important for devices adopting any form of development as well as facilitating hardware design through collaboration between all FPGA components.

The proposed Co-RLS design partitioned the conventional RLS between FIR constructed by the hardware components and embedded soft processor which also are contained in the FPGA platform. Instead of designing an RLS denoising system using FPGA hardware and its great complexity, the adaptation task is assigned to the soft processor which simplifies the co-RLS hardware architecture and makes the collection of FIR with adaptive processer as conventional RLS. The adaptation task is assigned to the soft processor, which calculates each P(n), and K(n) as

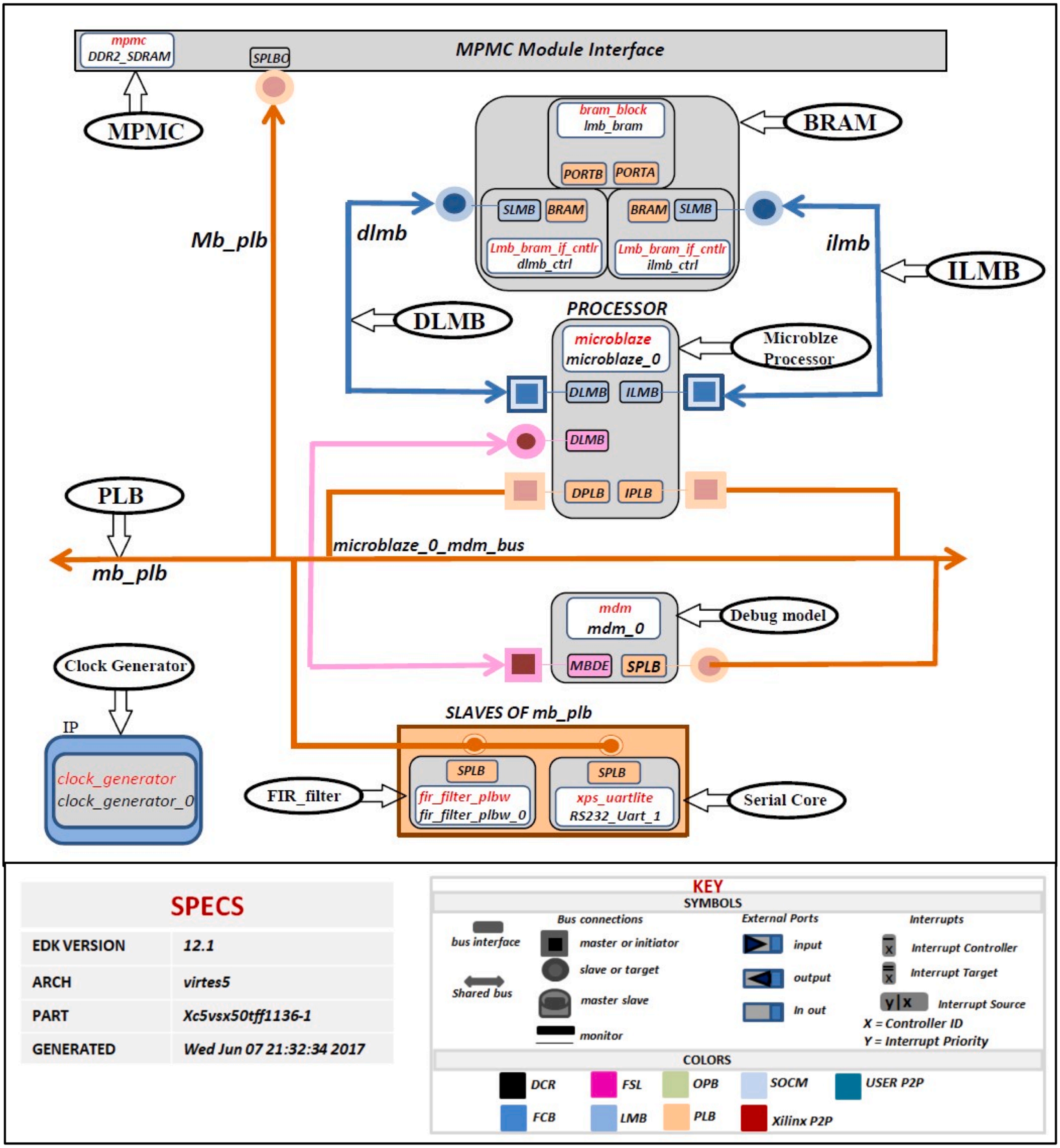

Fig. 4. Schematic diagram of the proposed co-design of an RLS filter sharing both hardware and programming (Microblaze Soft Processor) with an indication of interconnection with peripheral devices on the Virtex platform.

shown in Fig. 3.

The features of Microblaze™ soft core comprise 32-bit (general-purpose registers, instruction mode with two operands and three addressing styles), and a 32-bit address bus with a single pipeline. Adding Microblaze™ that is parameterized to permit selective enablement of add-ons. It can be configured using multiple buses such as the 32-PLB interface, or the LMB protocol synchronizes efficient Block-RAM transfers, while FSL provides fast, loose-flow communication, and XCL provides fast, controlled flow between memory controllers. External interface and cache, in addition to debugging internal interface used with the core of the microprocessor debugging unit (MDM) with the ability to track the interface for analysis [43]. FPGA manufacturers have sought to get the most out of their products by giving designers greater flexibility to achieve broader, more inclusive designs by including these gates with software wizards. Xilinx has created a Platform Builder Wizard (BSB) to create an embedded FPGA processor effectively, select types of memory, and control peripherals. Instructions size and type of data cache, optimization levels, the clock frequency of the processor and

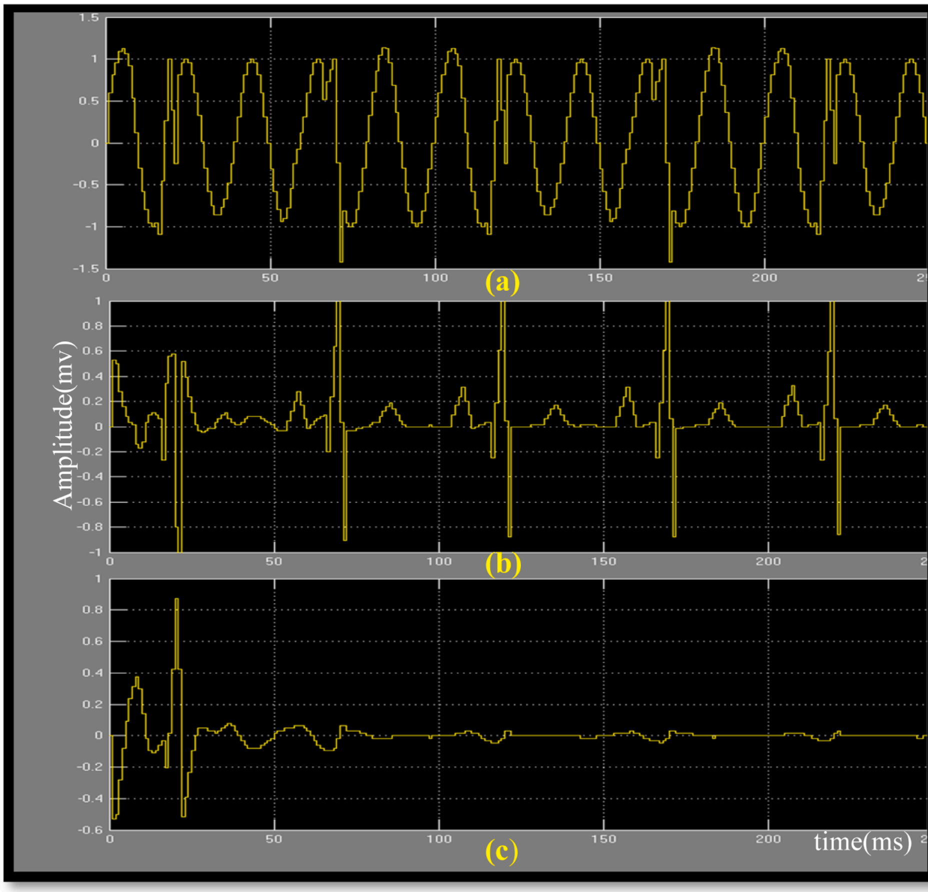

Fig. 5. Proposed de-noising results (a) ECG corrupted by Power line (b) clean ECG signal and (c) Error signal (8-taps for the FIR filter, λ=0.98 and δ=0.05).

local memory size are manipulated through GUI. The proposed RLS adaptive algorithm was written in C language on a Microblaze^{TM} soft processor according to the following steps:

1. Reading input samples and required signals from the file and storing them in SDRAM.
2. Determines filter output (by feeding the input samples with weights to the FIR filter) and then reads the output.
3. The affinity of the output samples is tested.
4. Computing k(n) and P(n) in the MicroBlaze soft processor.
5. Calculates the error if its value is at the minimum level or within the expected range (convergence), then there is no need to update the weights. Otherwise, return to step 2.
6. Finally, the XPS synthesis summary and the block diagram are created using the XPS via its GUI. Fig. 4 demonstrates the proposed Hardware/Software (HW/SW) system.

5. Result and discussion

Evaluation of the proposed HW/SW RLS architecture was tested on several noisy ECG signals from the MIT_BIH arrhythmia database available in (Moody and Mark, 2005) [44] and (MITBIH, 2022) [45]. Which includes 48 ECG recordings for half an hour at a 360 Hz sampling rate. Three types of noise added to each record in the database were done using MATLAB R2019 software and implemented on an Intel (R) Core i5-11th processor with a 64-bit operating system. Figs. 5, 6, and 7 show the resulting waves.

The proposed HW/SW filter was tested on diverse annals of MIT_BIH arrhythmia. The results illustrate the remarkable increase in the SNR by applying the proposed filter with three ECG noise types as shown in Figs. 8, 9, and 10 utilizing eight RLS taps. The average signal-to-noise (SNR) improvement of all recorders (100-150) is 89.78%. Filter tabs can be easily increased to any value using a system generator program, which raises the SNR, and the adaptation is simply done through the soft processor. Utilizing a floating-point instruction set in the assembly programming of Microblaze^{TM} increases the accuracy of adapting filter weights. The proposed collaboration of constructing RLS design excels in many aspects, the most important of which is its low consumption and the possibility of including it with heart signal sensors as is summarized in Table 2. Xilinx Power Analyzer tool was used to estimate the power consumed by conventional RSL (FPGA devices only) and the proposed Co-RLS design that uses a Microblaze processor to see how much it be reduced.

For 8-taps RLS adaptive filter the traditional RLS form needed (105) multiplier and (88) addition, with one division process. Giving the task of adaptation to the MicroBlaze^{TM} soft-processor reduces the complexity to FIR filter, that having eight multiplications and seven respectively. Which allowed to reduce the power consumed by a percentage 56.2 % for embedding with an ECG sensors.

6. Conclusion

In this paper, co-operation between hardware and software was implemented on Virtex-5. So, the software part can be easily changed to any other adaptive algorithm. Using the Microblaze^{TM} software processor in the FPGA eliminated the complexity of the RLS filter, making it extremely flexible even in terms of its length. Experimented results on the MIT-BIH arrhythmia database have a 67.37, 59.29, and 58.22dB SNR for 8-tap filter length and 69.37, 63.38, and 62.68dB when increasing filter length to 10-tap for nosing ECG by power line interference, baseline wandering, and mixing them in the third one. The low power consumption of the soft processor makes the proposed filter

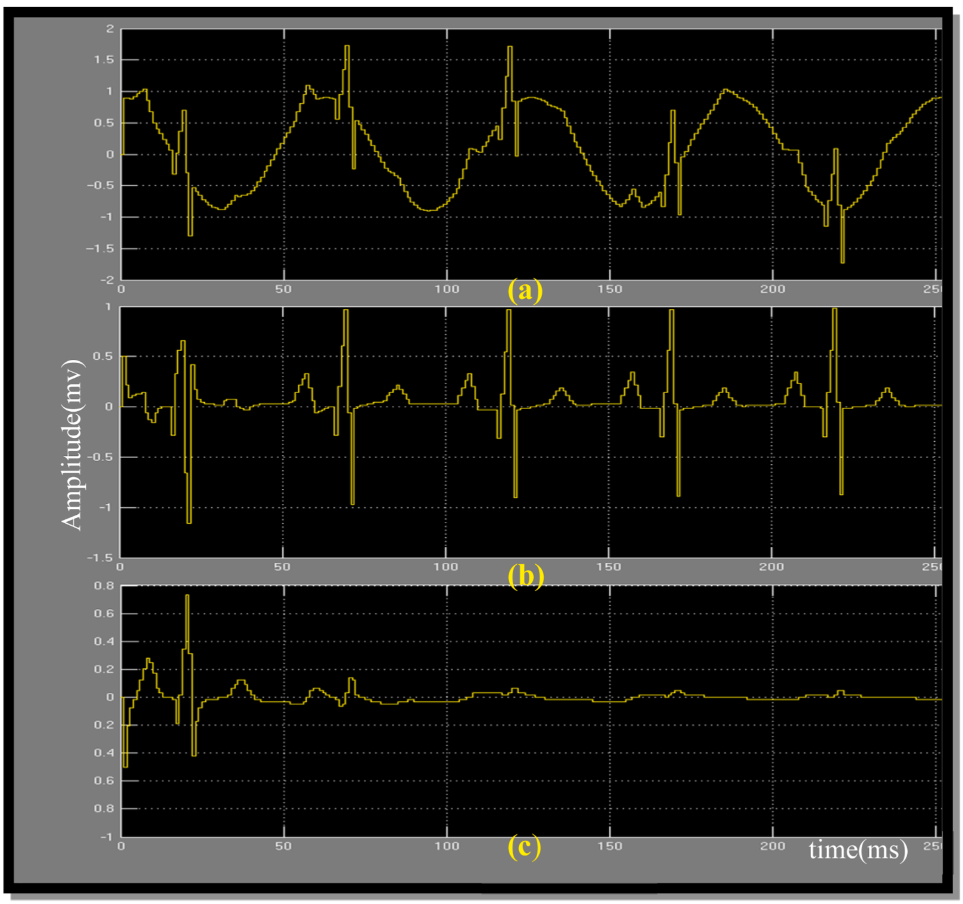

Fig. 6. Proposed de-noising results (a) ECG corrupted by Baseline wander (b) clean ECG signal and (c) Error signal (8 taps for the FIR filter, λ=0.98 and δ=0.05).

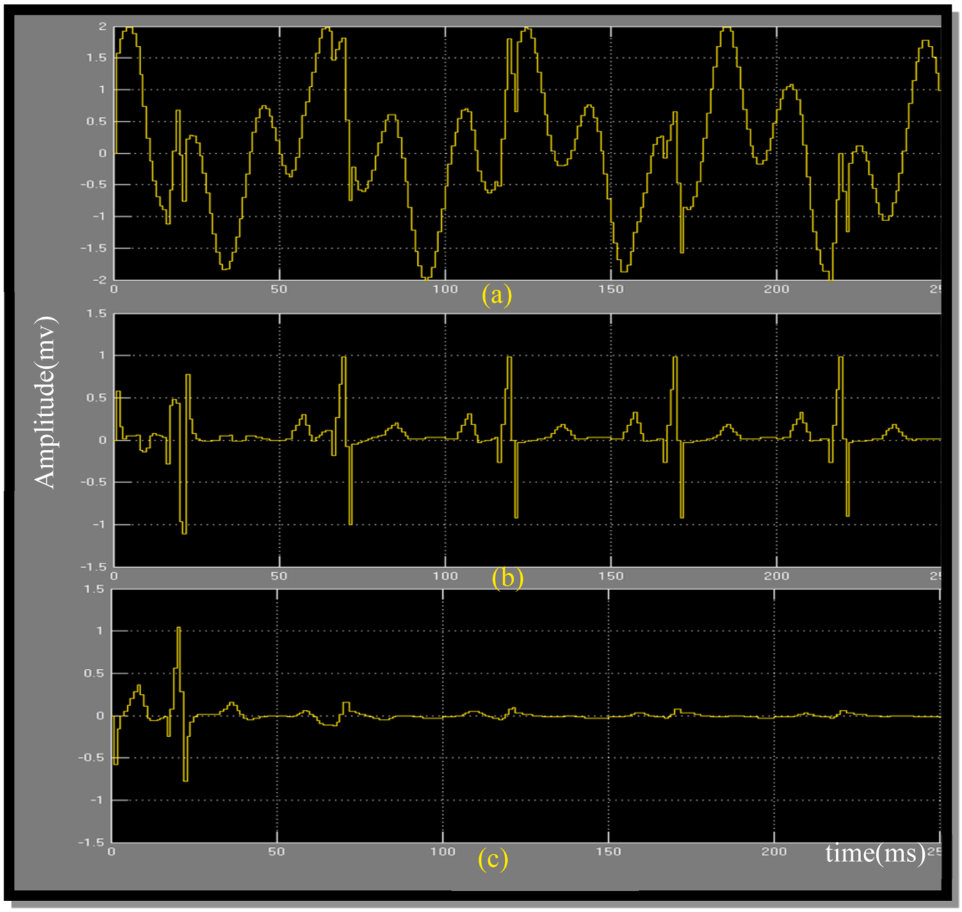

Fig. 7. Proposed de-noising results (a) ECG corrupted by Baseline wander and power line(b) clean ECG signal and (c) Error signal (8 taps for the FIR filter, λ=0.98 and δ=0.05).

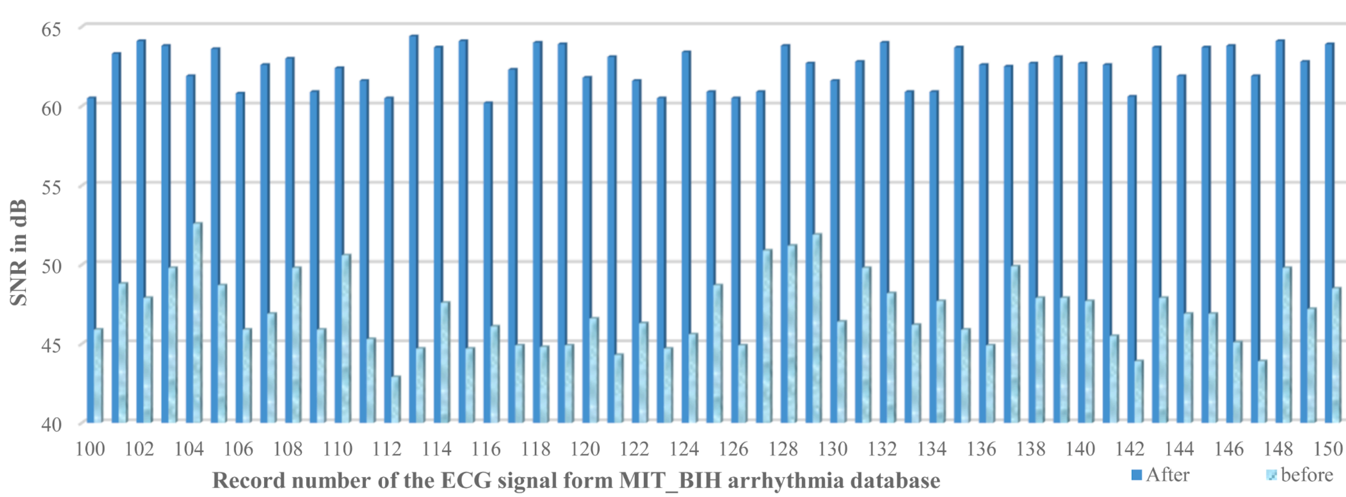

Fig. 8. SNR comparison before and after de-nosing the ECG signal from power line interference using the proposed Co-RLS design.

suitable to embed within ECG sensors for cleaning heart signals in real time.

Electroencephalogram (EEG) also has the same noise types so; the proposed work can be embedded with the EEG sensor for accurately measuring health signals in real-time in an IoT environment with lower power consumption. The proposed co-operation in constructing the filter reduces the computational complexity of the filter and makes it compatible for use in human body network sensors to measure vital parameters with high accuracy and longer life due to its low consumption.

Ethical approval

The research does not contain any experiments on living vertebrates or invertebrates. Not contain human participants or animals.

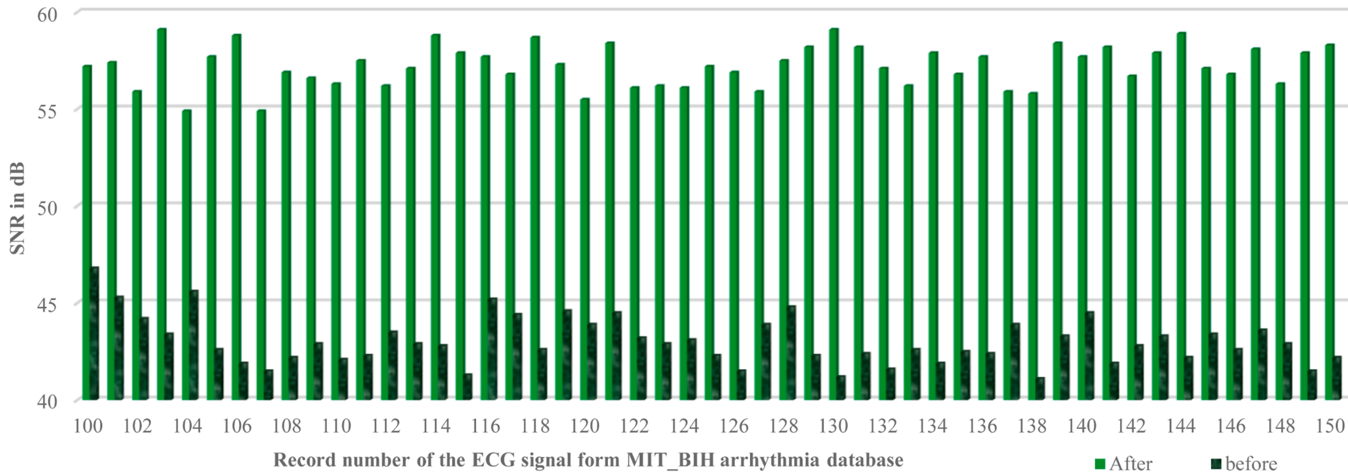

Fig. 9. SNR comparison before and after de-nosing the ECG signal from baseline wandering noise using the proposed Co-RLS design.

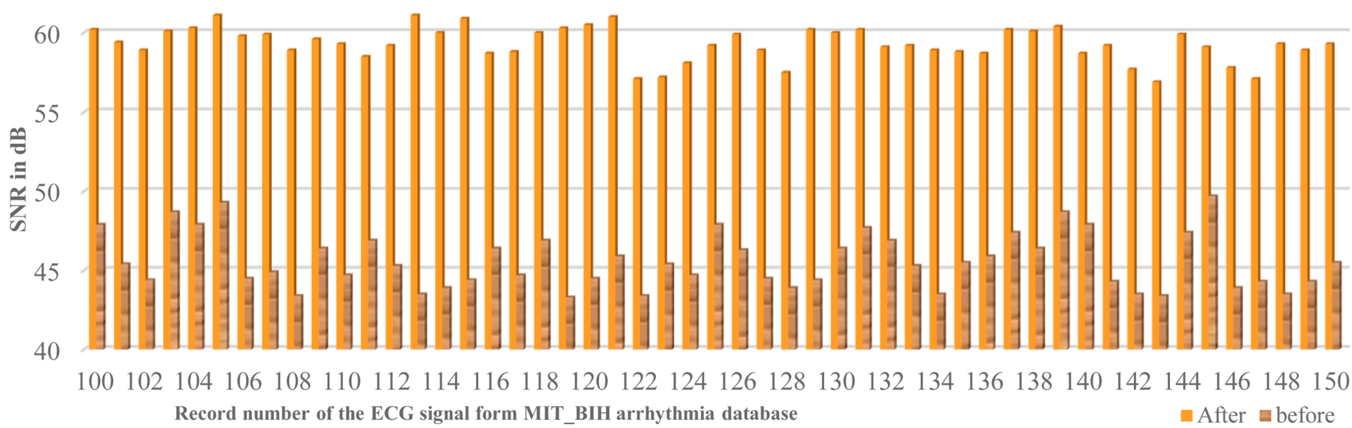

Fig. 10. SNR comparison before and after de-nosing the ECG signal from a power line with baseline wandering noise using the proposed Co-RLS design.

Table 2
Summarized Co-RLS design with recent de-nosing works.

Ref.	Dataset	Method	SNR dB				Real-System	Power
			PLI	BLW	MA	AV		
[6]	MIT-BIH	RLS	NA			19.9	Simulation	NA
[8]	MIT-BIH	LMS	9.47	9.47	9.32		only	NA
[10]	not mentioned	NN	30.43			10.7		NA
[21]	(101, 105, 117, 119, 121, 215, 223, and 230) of the MIT-BIH	Wavelet	62.6	NA				NA
[26]	4-ECG:MIT-BIH Normal Sinus Rhythm (Goldberger et al. 2003) and 4-ECG: MIT- BIH Arrhythmia (Moody andark 2001; Goldberger et al. 2003)	GAMNVE	56.3	NA				
[30]	75 records with reference annotations of fetal QRS	DCNN	NA			15		NA
[32]	MIT-BIH Arrhythmia	FIR	MSE:0.0501				Spartan-3E	RP
[34]	MIT-BIH Arrhythmia	WESBSF	16.1	NA	10.8		Simulation	NA
[46]	MIT-BIH Arrhythmia	DANet	NA	24.3	27.6	12.5	Simulation	NA
Popsoed	(100,101,...,150) MIT-BIH Arrhythmia	Co-RLS	63.4	63.38	62.7	23.5	Virtex-5	RP 56.2%

Note AV: Average Improving, NA: is Not Available, NN: Neural Network, GAMNVE: Genetic Algorithm Minimization of a new Noise Variation Estimate DCNN: Deep Convolutional Neural Networks, RP: Reduce Power, MSE: Mean Square Error, WESBSF: Wavelet Energy and Sub-Band Smoothing Filter.

Funding

The authors did not receive support from any organization.

CRediT authorship contribution statement

Ahlam Fadhil Mahmood: Writing – review & editing, Writing – original draft, Software, Methodology, Formal analysis, Data curation, Conceptualization. **Safaa N. Awny:** Writing – review & editing, Writing – original draft, Methodology, Investigation, Formal analysis, Conceptualization. **Ali Alameer:** Writing – review & editing, Writing – original draft, Supervision, Formal analysis.

Declaration of competing interest

The authors declare that they have no known competing financial interests or personal relationships that could have appeared to influence the work reported in this paper.

Data availability statements

The data that support the findings of this study are https://physionet.org/content/mitdb/1.0.0/ http://www.medteq.info/ECG_Data/MIT-BIH.zip.

Data availability

Data will be made available on request.

References

[1] P. Naseri, P. Amiri, H. Masihay-Akbar, S. Jalali-Farahani, D. Khalili, F. Azizi, Long-term incidence of cardiovascular outcomes in the middle-aged and elderly with different patterns of physical activity: Tehran lipid and glucose study, BMC. Public Health 20 (1654) (2020) 10, https://doi.org/10.1186/s12889-020-09747-6.

[2] S. Qin, L. Huang, J. Zhou, H. Wang, Q. Li, H. Wu, J. Wu, Prevalence and related risk factors associated with coronary heart disease (CHD) among middle-aged and elderly patients with vision impairment (VI), Int. J. Gen. Med. 14 (2021) 6125–6133. https://pubmed.ncbi.nlm.nih.gov/346114427/.

[3] A. Groenewegen, F.H. Rutten, A. Mosterd, A.W. Hoes, Epidemiology of heart failure, Eur. J. Heart. Fail. (2020), https://doi.org/10.1002/ejhf.1858.

[4] P.R. Rijnbeek, G. Herpen, M.L. Bots, S. Man, N. Verweij, A. Hofman, H. Hillege, M. E. Numans, C.A. Swenne, J.C.M. Witteman, J.A. Kors, Normal values of the electrocardiogram for ages 16–90 years. J. Electrocardiol., Sci. Direct, 2014, p. 9, https://doi.org/10.1016/i.jelectrocard.2014.022.

[5] G. Lippi, F. Sanchis-Gomar, Global epidemiology and future trends of heart failure, AMe Med. J. 5 (15) (2020) 6. https://amj.amegroups.com/article/view/5475/html.

[6] X. An, G.K. Stylios, Comparison of motion artefact reduction methods and the implementation of adaptive motion artefact reduction in Wearable Electrocardiogram Monitoring, Sensors 20 (5) (2020) 1468. https://pubmed.ncbi.nlm.nih.gov/32155984/.

[7] S. Chatterjee, R.S. Thakur, R.N. Yadav, L. Gupta, D.K. Raghuvanshi, Review of noise removal techniques in ECG signals, IET Signal Process. 14 (9) (2020) 569–590, https://doi.org/10.1049/iet-spr.2020.0104.

[8] F. Mohaddes, R. Silva, F.P. Akbulut, Y. Zhou, A. Tanneeru, E. Lobaton, B. Lee, V. Misra, A pipeline for adaptive filtering and transformation of noisy left-arm ECG to its surrogate chest signal, Electronics. (Basel) 9 (866) (2020) 17. https://www.mdpi.com/2079-9292/9/5/866.

[9] M. Wu, Y. Lu, W. Yang, S.Y. Wong, A Study on Arrhythmia via ECG Signal Classification Using the Convolutional Neural Network, Front. Comput. Neurosci. 14 (2021) 10, https://doi.org/10.3389/fncom.2020.564015, article 564015.

[10] N. Sasirekha, P.V. Karthick, T. Premakumari, J. Harirajkumar, S. Aishwarya, Noise Removal in ECG Signal Using Digital Filters, Eur. J. Mol. Clin. Med. 07 (02) (2020) 5145–5149. https://ejmcm.com/article_3136_4bd12a4487b4eb3d4e2a374b5dac3f88.pdf.

[11] M. Zhang, G. WeiI, An integrated EMD adaptive threshold denoising method for reduction of noise in ECG, PLoS. One 15 (7) (2020) e0235330. https://journals.plos.org/plosone/article?id=10.1371/journal.pone.0235330.

[12] R. Biroka, R. Kapoorb, M.S. Choudhry, ECG denoising using artificial neural networks and complete ensemble empirical mode decomposition, Turkish J. Comput. Math. Educ. 12 (2) (2021) 2382–2389. https://turcomat.org/index.php/turkbilmat/article/view/2033.

[13] J. Moini, Anatomy & Physiology, Chapter Thirteen-The Cardiovascular System, Jones & Bartlett Publishers, 2013 third edition, http://samples.jblearning.com/9781284175073/9781284175073_Boling_CH02_SECURE.pdf.

[14] S. Aron, MSC. Thesis, Electrical and Computer Engineering, Waterloo, Ontario, Canada, 2013.

[15] N. Prashar, M. Sood, S. Jai, Dual-tree complex wavelet transform technique-based optimal threshold tuning system to deliver denoised ECG signal, Trans. Inst. Meas. Control (2020) 16, https://doi.org/10.1177/0142331219895708.

[16] L. Xie, Z. Li, Y. Zhou, Y. He, J. Zhu, Computational diagnostic techniques for elec-signal analysis, Sensors 20 (6318) (2020) 32, https://doi.org/10.3390/s20216318.

[17] M. Venkateswarlu, S.N. Bhavanam, A survey on noise suppression in ECG Signals using Filter Banks and Wavelet Processing Techniques, J. Crit. Rev. 7 (09) (2020), https://doi.org/10.1109/CSNT.2013.22. ISSN-2394-5125.

[18] C. Lastre-Dom-nguez, Y.S. Shmaliy, O. Ibarra-Manzano, J. Munoz-Minjares, L. J. Morales-Mendoza, ECG signal denoising and features extraction using unbiased FIR smoothing, Hindawi BioMed Res. Int. 2019 (2019) 16, https://doi.org/10.1155/2019/2608547. Article ID 2608547.

[19] C. Ngo, C. Munoz, M. Lueken, A. Hülkenberg, C. Bollheimer, A. Briko, A. Kobelev, S. Shchukin, S. Leonhardt, A wearable, multi-frequency device to measure muscle activity combining simultaneous electromyography and electrical impedance myography, Sensors 22 (1941) (2022) 16, https://doi.org/10.3390/s22051941.

[20] J. Jeong, W. Lee, Y. Kim, A real-time wearable physiological monitoring system for home-based healthcare applications, Sensors 22 (104) (2022) 14, https://doi.org/10.3390/s22010104.

[21] I. Houamed, L. Saidi, F. Srair, ECG signal denoising by fractional wavelet transform thresholding, Res. Biomed. Eng. 36 (2020) 349–360, https://doi.org/10.1007/s42600-020-00075-7.

[22] D. Zhang, S. Wang, F. Li, S. Tian, J. Wang, X. Ding, R. Gong, An Efficient ECG Denoising Method Based on Empirical Mode Decomposition, Sample Entropy, and Improved Threshold Function, Hindawi Wirel. Commun. Mobile Comput. 2020 (2020) 360, https://doi.org/10.1155/2020/8811962. Article ID 8811962.

[23] A. Giorgio, C. Guaragnella, D.A. Giliberti, Improving ECG signal denoising using wavelet transform for the prediction of malignant arrhythmias, Int. J. Med. Eng. Inf. 12 (2) (2020) 135–150, https://doi.org/10.1504/IJMEI.2020.106898.

[24] P. Madana, V. Singha, D.P. Singha, M. Diwakara, A. Kish, Denoising of ECG signals using weighted stationary wavelet total variation, Biomed. Signal. Process. Control 73 (2022) 103478, https://doi.org/10.1016/j.bspc.2021.103478.

[25] A. Rasti-Meymandi, A. Ghaffari, A deep learning-based framework For ECG signal denoising based on stacked cardiac cycle, Biomed. Signal. Process. Control 71 (2022) 103275, https://doi.org/10.1016/j.bspc.2021.103275.

[26] R.N. Vargas, A.C.P. Veiga, Electrocardiogram signal denoising by a new noise variation estimate, Res. Biomed. Eng. 36 (2020) 13–20, https://doi.org/10.1007/s42600-019-00033-y.

[27] Y. Su, C.-C. Jay Kuo, Recurrent neural networks and their memory behavior: a survey, APSIPa Trans. Signal. Inf. Process. 11 (2022) 38, https://doi.org/10.1561/116.00000123, 2022e26.

[28] A. Darmawahyuni, S. Nurmaini, M.N. Rachmatullah, B. Tutuko, A.I. Sapitri, F. Firdaus, A. Fansyuri, A. Predyansyah, Deeplearning-based electrocardiogram rhythm and beat features for heart abnormality classification, Peer J. Comput. Sci. 8 (2022) 26, https://doi.org/10.7717/peerj-cs.825, e825.

[29] Y. Su, C.-C.J. Kuo, On extended long short-term memory and dependent bidirectional recurrent neural network, Neurocomputing. 356 (2019) 151–161, https://doi.org/10.1016/j.neucom.2019.04.044.

[30] E. Fotiadou, R. Vulling, Multi-channel fetal ECG denosing with deep convolutional neural networks, Front. Pediatr. 8 (2020) 13, https://doi.org/10.3389/fped.2020.00508, article 508.

[31] H.B. Aboh Hamid, X. Liu, Adaptive model predictive control scheme for partially internal thermally coupled air separation column, Res. Eng. (2024) 102678, https://doi.org/10.1016/j.rineng.2024.102678.

[32] P.C. Bhaskara, M.D. Uplane, High frequency electromyogram noise removal from electrocardiogram using FIR low pass filter based on FPGA, ScienceDirect, Procedia Technol. 25 (2016) 497–504, https://doi.org/10.1016/j.protcy.2016.08.137.

[33] S. Särkkä, Bayesian Filtering and smoothing, Cambridge University Press, 2014, https://doi.org/10.1017/CBO9781139344203.

[34] D. Zhang, S. Wang, F. Li, J. Wang, A.K. Sangaiah, V.S. Sheng, X. Ding, An ECG signal de-noising approach based on wavelet energy and sub-band smoothing filter, Appl. Sci. 9 (2019) 4968, https://doi.org/10.3390/app9224968.

[35] S. Poungponsri, X. Yu, Electrocardiogram (ECG) signal modeling and noise reduction using wavelet neural networks, in: Proceedings of the IEEE International Conference on Automation and Logistics Shenyang, China, 2009, https://doi.org/10.1109/ICAL.2009.5262892.

[36] L. Dogariu, C. Stanciu, C. Elisei-Iliescu, C. Paleologu, J. Benesty, S. Ciochin, Tensor-based adaptive filtering algorithms, Symmetry. (Basel) 13 (481) (2021) 27, https://doi.org/10.3390/sym130.30481.

[37] Z.A. Khan, T. Hussain, U. Zabit, M. Usman, E. Ayguade, PH-RLS: a parallel hybrid recursive least square algorithm for self-mixing interferometric laser sensor, IET Optoelectronics (1–9) (2021), https://doi.org/10.1049/ote2.12021.

[38] P. Rakesh, T.K. Kumar, A novel RLS based adaptive filtering method for speech enhancement, World Acad. Sci., Eng. Technol. Int. J. Electr. Commun. Eng. 9 (2) (2015) 176–181, https://doi.org/10.5281/zenodo.1099384.

[39] Virtex–5 FPGA User Guide, UG190 (v5.4), 2012. http://www.gstitt.ece.ufl.edu/courses/fall12/eel4720_5721/reading/v5userguide.pdf.

[40] ML505/ML506/ML507 Getting Started Tutorial For ML505/ML506/ML507 Evaluation Platforms, UG348, (v3.0.2) 2008. http://www.bdtic.com/download/XILINX/ug348.pdf.

[41] Embedded Processor Block in Virtex-5 FPGAs Reference Guide UG200 (v1.8) 2010. https://docs.xilinx.com/v/u/en-US/ug200.

[42] MicroBlaze Processor Reference Guide 3 UG984 (v2021.2), 396, 2021. https://www.xilinx.com/content/dam/xilinx/suport/documents/sw_manuals/xilinx2021_2/ug984-vivado-microblaze-ref.pdf.

[43] V.A. Akpan, Hard and soft embedded FPGA processor systems design: design considerations and performance comparisons, Int. J. Eng. Technol. 3 (11) (2013). https://www.researchgate.net/.

[44] https://physionet.org/content/mitdb/1.0.0/.

[45] http://www.medteq.info/ECG_Data/MITBIH.zip.

[46] H. Lin, R. Liu, Z. Liu, ECG signal denoising method based on disentangled autoencoder, Electronics. (Basel) 12 (2023) 1606, https://doi.org/10.3390/electronics12071606.